Applied Physics Letters

Plasma instability in graphene field-effect transistors with a shifted gate

Cite as: Appl. Phys. Lett. **121**, 143502 (2022); https://doi.org/10.1063/5.0111560
Submitted: 19 July 2022 • Accepted: 16 September 2022 • Published Online: 06 October 2022

J. Crabb, X. Cantos Roman, J. M. Jornet, et al.

AIP Publishing

Applied Physics Letters ARTICLE scitation.org/journal/apl

Plasma instability in graphene field-effect transistors with a shifted gate

Cite as: Appl. Phys. Lett. **121**, 143502 (2022); doi: 10.1063/5.0111560
Submitted: 19 July 2022 · Accepted: 16 September 2022 ·
Published Online: 6 October 2022

J. Crabb,[1,a)] X. Cantos Roman,[1] J. M. Jornet,[1] and G. R. Aizin[2]

AFFILIATIONS

[1]Department of Electrical and Computer Engineering, Northeastern University, Boston, Massachusetts 02215, USA
[2]Kingsborough College, The City University of New York, Brooklyn, New York 11235, USA

[a)]Author to whom correspondence should be addressed: crabb.j@northeastern.edu

ABSTRACT

We present detailed numerical analysis of the Dyakonov–Shur (DS) plasma instability in a DC biased graphene field-effect transistor (FET) with the gate shifted with respect to the middle of the transistor conducting channel. We show that the geometric asymmetry is sufficient to trigger the DS instability in the two-dimensional electron gas in the transistor channel. We demonstrate sustained plasma oscillations in the instability end point and analyze the properties of these oscillations for different positions of the gate and at different values of other physical and geometric FET parameters. The obtained results show the possibility of designing a tunable on-chip source of terahertz electromagnetic radiation based on the graphene FET with shifted gate.

Recent years have shown the highest increase in demand for faster internet due to the exponential growth in the number of online-connected applications and their number of users.[1] To meet the projected demand, wireless data rates in the terabit per second range are required. These rates are achievable with higher bandwidths offered in the terahertz (THz) band (0.1–10 THz) of the electromagnetic (EM) spectrum.[2] Currently, there are a number of applications based on the short-range wireless communications in the THz domain, such as wireless networks on chip (WNoC),[3] internet of nano-things,[4] and nanosensor networks.[5] However, the progress in these areas is hampered by the lack of a compact, efficient, room-temperature operating source of THz EM radiation.

One of the most promising approaches for the development of such a source is to use electron plasma oscillations in the two-dimensional (2D) electron channel of field-effect transistors (FETs). Recent experiments in graphene FETs demonstrated high-quality electron plasma oscillations at room temperatures.[6,7] The frequency of the 2D plasma oscillations lies in the THz domain. The compact FET size, its compatibility with planar CMOS technology, and the possibility of external control of the plasma frequency make FETs a very attractive candidate for the development of a tunable THz source of EM radiation.

The main challenge in the development of a THz source based on the plasmonic FET is the conversion of the plasma oscillations in the FET electron channel into the EM signal. The physical mechanism for this conversion was proposed by Dyakonov and Shur (DS) in Ref. 8. The authors theoretically demonstrated that in a FET biased by a DC, the amplitude of plasma waves may exponentially increase after multiple reflections from the source and the drain ends of the plasmonic cavity formed in the FET channel. This effect, known as the Dyakonov–Shur (DS) instability, occurs if asymmetric boundary conditions for plasma wave reflections are imposed at opposite ends of the plasmonic cavity. Namely, the impedance between the Ohmic contact and the gate at one side of the FET cavity (the drain side) should be larger than the one at the opposite side (the source side) when a DC flows from the drain to the source. In the instability end point, stationary sustained plasma oscillations are developed in the channel, and the energy supplied by the DC is balanced by Joule losses and radiation.[9–11] In the theory developed in Ref. 8, ideal boundary conditions with the gate–source impedance $Z_{gs} = 0$ and the gate–drain impedance $Z_{gd} = \infty$ were used. However, it was shown later[9,12,13] that the DS instability takes place at any finite Z_{gs} and Z_{gd}, provided that $Z_{gd} > Z_{gs}$ and Joule losses are sufficiently small.

Difficulties in experimental demonstration of the DS instability are mostly connected with practical implementations of the asymmetric boundary conditions. In early experimental works,[14] the asymmetry provided by shorting the source and gate contacts and depleting the semiconductor FET channel near the drain was insufficient, and only weak broadband THz radiation at cryogenic temperatures was observed. In later works,[15] the FET asymmetry was improved by

asymmetrically placing the gate contact with respect to the source and the drain contacts of the FET, and resonant THz emission at plasma frequencies tunable by the gate voltage was observed. Very recently, the semiconductor FET with engineered structural asymmetry has been designed in order to study the asymmetry effect on plasma instability.[16] Transport measurements in these structures demonstrated sustainable plasma oscillations in the FET cavity consistent with the DS instability, though THz emission measurements were not attempted in this work. A unified approach to evaluating the plasma instability in current-biased FET channels without mirror symmetry was developed in Ref. 17. Furthermore, the effect of geometric asymmetry in the gate position along the FET channel on the detection of THz radiation by graphene FETs was recently measured in Ref. 18.

In this Letter, we present a systematic theoretical study of the DS instability in the graphene FET with a shifted gate. Since the impedances Z_{gs} and Z_{gd} are capacitive in nature, positioning the gate at different distances from the source and the drain contacts results in different values of Z_{gs} and Z_{gd} and may trigger the DS plasma instability. The proposed FET architecture is shown in Fig. 1. The graphene channel of length L is sandwiched between the dielectric substrate of thickness l and the barrier of thickness d separating the channel from the metal gate contact. The source and the drain metal contacts are attached on either side of the structure. The gate contact of length $L_g < L$ can be positioned arbitrarily along the channel, thus providing the required geometric asymmetry. (This geometry differs from the geometry of the partly gated channel considered in Ref. 17, where the gate of variable length was placed next to one of the side contacts.) We assume that a DC bias current I_{ds} flows in the FET channel between the drain and source contacts, and a constant gate voltage V_{gs} controls the equilibrium electron density in the channel under the gate, n_g, whereas the electron density in ungated parts of the channel, n_u, remains constant. The equilibrium electron density in the channel $n_0(x)$ is modeled as

$$n_0(x) = n_u + (n_u - n_g)\left(\frac{1}{1+e^{\frac{x-x_L}{w}}} - \frac{1}{1+e^{\frac{x-x_R}{w}}}\right), \tag{1}$$

where $x_L(x_R)$ are x-coordinates of the left (right) edge of the gate contact as shown in Fig. 1, so that $x_R - x_L = L_g$, and $2w$ is the length of the transition region between gated and ungated parts of the channel. An example of the normalized equilibrium electron density distribution $n_0(x)/n_u$ as a function of x/L with $n_g = n_u/3$, $L_g = 0.5L$, and $w = L_g/25$ is shown in the inset in Fig. 1.

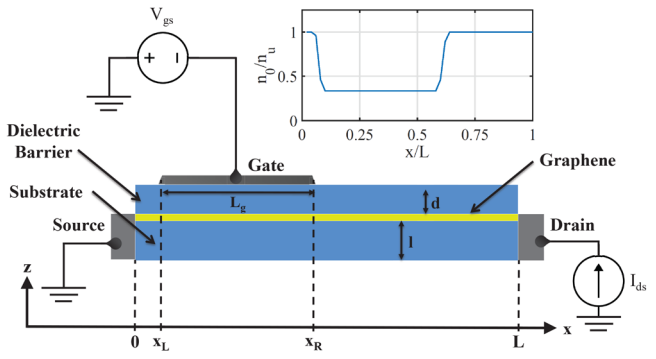

FIG. 1. Schematic of the graphene FET with a shifted gate. Inset: normalized equilibrium electron density distribution in the FET channel from Eq. (1) with $L_g = 0.5L$, $x_L = 0.08L$, $w = L_g/25$, and $n_g = n_u/3$.

The electron transport in the graphene FET channel can be described within the hydrodynamic model used in a number of publications.[19–24] In this model, the equation of continuity connects the electron density $n(x, t)$ and the hydrodynamic velocity $v(x, t)$ in the channel as

$$\frac{\partial n}{\partial t} + \frac{\partial j}{\partial x} = 0, \tag{2}$$

where $j = nv$ is the electron flow density. The electron dynamics in the channel is described by the Euler equation. The Euler equation for massless 2D Dirac fermions in the DC-biased graphene layer at arbitrary values of the velocity v was recently derived in Ref. 11 and has the following form:

$$\frac{2-\beta^2}{2(1-\beta^2)}\frac{\partial v}{\partial t} + \frac{v_F^2(1-\beta^2)}{2n}\frac{\partial n}{\partial x} + \frac{\beta^2}{2(1-\beta^2)}v\frac{\partial v}{\partial x} + \frac{v_F(1-\beta^2)^{1/4}}{\sqrt{\pi}\hbar\sqrt{n}}eE_x + \frac{(v-v_0)(1-\beta^2)^{1/4}}{\tau}\sqrt{\frac{n_0}{n}} = 0. \tag{3}$$

Here, $\beta = \frac{v}{v_F}$, n_0 is the equilibrium electron density, v_0 is the drift velocity due to stationary electron flow $j_0 = n_0 v_0 = const$ between the source and the drain, τ is the electron momentum relaxation time, $v_F = 1.5 \times 10^6\ \mathrm{m\,s^{-1}}$ is the electron Fermi velocity in graphene, and $-e$ is the electron charge. The self-consistent electric field E_x in Eq. (3) is induced by the charged fluctuations in the electron system. Equation (3) was derived for uniform electron systems with $n_0 = const$ but can be generalized to electron channels with non-uniform equilibrium electron density $n_0(x)$ considered in this paper. In the latter case, Eq. (3) remains valid, but the electric field E_x now also includes a static built-in electric field E_{0x} producing the non-uniform equilibrium electron density distribution. This electric field can be easily found from Eq. (3) in the stationary limit when $n(x,t) = n_0(x)$ and $E_x(x,t) = E_{0x}(x)$. Splitting the total field E_x in Eq. (3) as $E_x = E_{0x} + E_x^{ind}$, where E_x^{ind} is the induced electric field, we finally obtain

$$(2-\beta^2)\frac{\partial j}{\partial t} + 2\beta v_F\frac{\partial j}{\partial x} + (1-2\beta^2)v_F^2\frac{\partial n}{\partial x} + \frac{2v_F(1-\beta^2)^{5/4}}{\sqrt{\pi}\hbar}\sqrt{n}eE_x^{ind} - (1-2\beta^2)\left(\frac{1-\beta^2}{1-\beta_0^2}\right)^{5/4}v_F^2\sqrt{\frac{n}{n_0}}\frac{dn_0}{dx} + \frac{2(j-\beta_0 v_F n)(1-\beta^2)^{5/4}}{\tau}\sqrt{\frac{n_0}{n}} = 0, \tag{4}$$

where $\beta_0 = \frac{j_0}{n_0 v_F}$. The electric field $E_x^{ind}(x,t)$ can be found from the system of Maxwell's equations

$$\nabla \times \boldsymbol{E}^{ind} = -\mu_0\frac{\partial \boldsymbol{H}^{ind}}{\partial t}, \qquad \nabla \times \boldsymbol{H}^{ind} = -e(j-j_0)\delta(z)\hat{\mathbf{x}} + \varepsilon\varepsilon_0\frac{\partial \boldsymbol{E}^{ind}}{\partial t}, \tag{5}$$

where $\boldsymbol{E}^{ind} = E_x^{ind}\hat{\mathbf{x}} + E_z^{ind}\hat{\mathbf{z}}$ and $\boldsymbol{H}^{ind} = H_y^{ind}\hat{\mathbf{y}}$ are the electric and magnetic components of the EM field induced by the electric current $-e(j-j_0)\delta(z)\hat{\mathbf{x}}$ in the channel. Equations (2), (4), and (5) form the closed system of equations, provided that the profile $n_0(x)$ is given

and should be solved self-consistently in order to describe the collective plasma excitations in the 2D graphene channel and accompanying electromagnetic radiation generated in the instability regime.[9–11]

We solved the system of equations (2), (4), and (5) numerically using our in-house developed multiphysics simulation platform, providing simultaneous self-consistent solutions of the hydrodynamic and Maxwell's equations. Recently, this platform was successfully used for modeling the DS instability in both semiconductor[9,16] and graphene[11,25] FETs with externally imposed ideal as well as non-ideal boundary conditions defining the values of Z_{gs} and Z_{gd}. In this study, no boundary conditions were artificially imposed at the ends of the FET channel. This approach is more consistent because the capacitive links between the metal source, drain, and gate contacts are inherently included in the system of Maxwell's equations describing the whole transistor structure.

In our numerical simulations, we used the channel length $L = 1\,\mu$m, gate length $L_g = 0.5\,\mu$m, and thicknesses of the barrier layer and the substrate $d = 20$ nm and $l = 400$ nm, respectively. The relative electric permittivity of the dielectric material is assumed to be $\varepsilon = 3.8$, and all transistor terminals were assigned very high conductivity making them ideal metal contacts. We assumed that the 2D electron gas in the graphene channel is depleted under the gate with electron density $n_{0,g} = 2 \times 10^{16}\,\mathrm{m}^{-2}$, and the electron density in the ungated parts of the channel $n_{0,u} = 6 \times 10^{16}\,\mathrm{m}^{-2}$. The length of the transition region between gated and ungated parts of the channel in Eq. (1) was taken as $w = 20$ nm.

In Fig. 2, we present our results demonstrating the temporal evolution of the plasma oscillations developing after initial random local perturbation of the electric current. In this calculation, we use the value of the electron drift velocity under the gate $v_0 = 2.8 \times 10^5\,\mathrm{m\,s}^{-1}$ and the electron momentum relaxation time $\tau = 2.3$ ps. In Fig. 2(a), we show the temporal evolution of the plasmonic signal in the FET channel with the gate in the immediate vicinity of the source contact, so that $x_L = 20$ nm, and the drift velocity v_0 pointing in the source-to-drain direction as indicated in the inset atop of the graph. In this FET configuration, the impedance Z_{gd} is much larger than Z_{gs}, and for the given direction of the electron drift, the DS instability should develop in the channel provided that the instability increment $v_0/L_g (\sim 5.6 \times 10^{11}\,\mathrm{s}^{-1})$ exceeds the plasmon damping $1/\tau (\sim 4.3 \times 10^{11}\,\mathrm{s}^{-1})$.[8,11] This conclusion is confirmed by the results shown in Fig. 2(a). In the instability end point reached in about 20 ps after the initial perturbation, the sustained plasma oscillations are developed and maintained in the channel.

Our numerical simulations (not shown here) demonstrate that for the values of v_0 smaller than the threshold drift velocity $v_0^{th} \approx 2.7 \times 10^5\,\mathrm{m\,s}^{-1}$, the plasma oscillations are damped. This numerically found value of the threshold drift velocity is larger than the one predicted for the ideal boundary conditions:[8,11] $L_g/\tau \approx 2.2 \times 10^5\,\mathrm{m\,s}^{-1}$. This result is in compliance with the theoretical results in Refs. 9, 12, and 13, predicting the increase in v_0^{th} for the non-ideal boundaries. Also, numerical calculations of v_0^{th} made at different values of the electron density under the gate, $n_{0,g}$, did not show any dependence of v_0^{th} on $n_{0,g}$ (with numerical accuracy of $\pm 2\%$), indicating that the boundary impedances weakly depend on the electron density change at the interface between the gated and ungated parts of the channel.

The fundamental frequency of the sustained oscillations is about 1.3 THz as follows from the spectral content of the plasma oscillations shown in Fig. 2(a) next to the graph. The theoretical value of the fundamental plasma frequency under ideal boundary conditions can be found as $f_0 = v_p/4L_g$, where $v_p = \left(v_F^2/2 + e^2\sqrt{n_g}dv_F/\sqrt{\pi}\varepsilon\varepsilon_0\hbar\right)^{1/2}$ is the plasma velocity in graphene.[22,23] This expression yields $f_0 = 2.15$ THz, which is markedly larger than our numerical value. The difference between these two values of f_0 is due to the non-ideal boundary conditions used in the numerical simulation. The finite values of Z_{gs} and Z_{gd} result in a decrease in the resonant plasma frequency.[9] In Fig. 2(b), the same calculation as in Fig. 2(a) but with opposite direction of the drift velocity is shown. In this case, the plasma oscillations are damped as expected.[8,11] This confirms the origin of the plasma instability as the DS instability. The last conclusion is further confirmed in Fig. 2(c) where temporal evolution of the

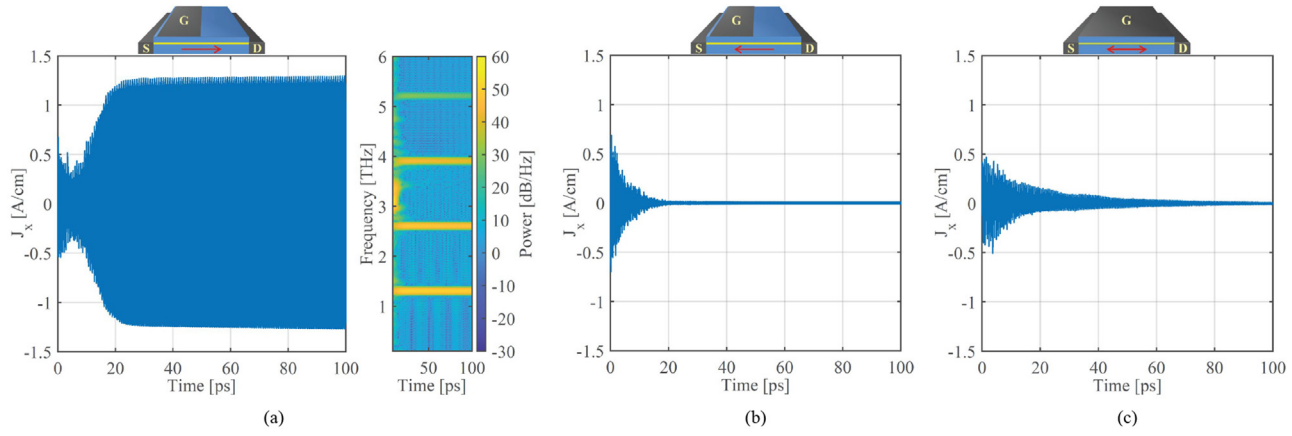

FIG. 2. (a) Temporal evolution of the plasmonic current density in the current-biased graphene FET channel with a shifted gate ($x_L = 20$ nm, $L_g = 0.5L$) and positive direction of the drift velocity. The current spectral content is shown to the right of the current plot. (b) The same plot as in (a) but for the negative drift velocity. (c) The same plot as in (a) but with the gate extending from the source to the drain and both directions of the drift velocity. In all plots $L = 1\,\mu$m, $v_0 = 2.8 \times 10^5\,\mathrm{m\,s}^{-1}$, $\tau = 2.3$ ps, $n_u = 6 \times 10^{16}\,\mathrm{m}^{-2}$, and $n_g = n_u/3$. Insets: schematics of the device configuration with arrows indicating the direction of the drift velocity.

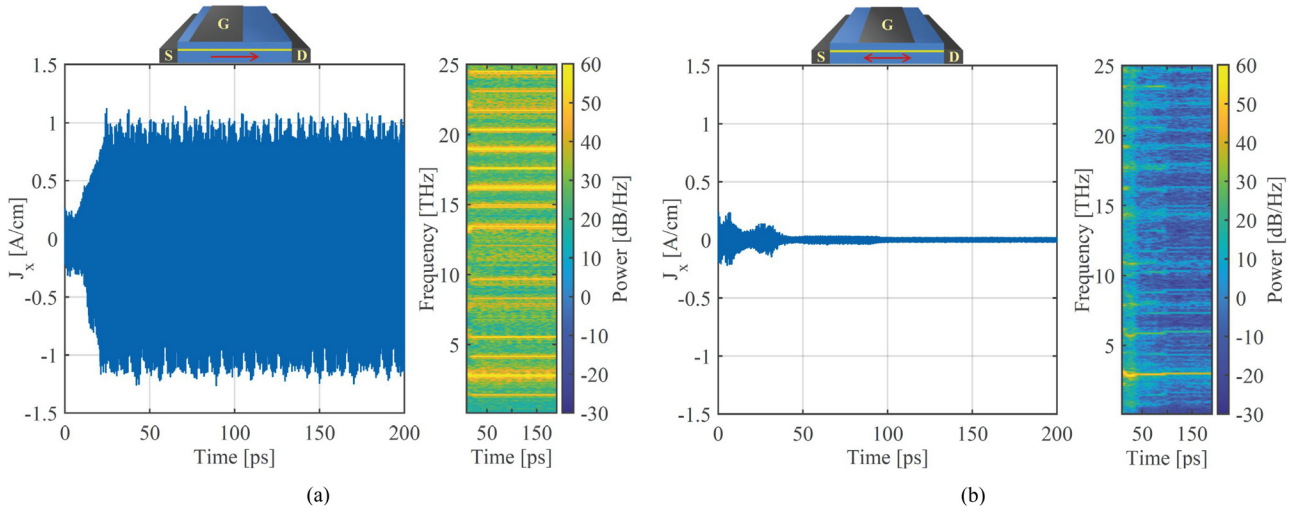

FIG. 3. Temporal evolution of the plasmonic current density in the current-biased graphene FET channel with the gate shifted to different positions: (a) $x_L = 80$ nm; (b) $x_L = 260$ nm. All other parameters are the same as in Fig. 2. The current spectral content is shown to the right of the current plots. Insets: schematics the device configuration with arrows indicating the direction of the drift velocity.

plasma oscillations is considered in the FET configuration where the gate extends from the source to the drain for the same values of the parameters as in Figs. 2(a) and 2(b). In this case, the system is symmetric ($Z_{gs} = Z_{gd}$), and plasma oscillations are damped for both directions of the drift velocity.

When the gate shifts toward the middle of the channel, the difference between Z_{gs} and Z_{gd} decreases, reducing the DS instability increment.[9,12] This results in the reduction in signal amplitude shown in Fig. 3(a), where calculations of the plasmonic signal were performed for the gate positioned closer to the middle of the channel with $x_L = 80$ nm. The weakened plasmonic signal with a fundamental frequency around 1.3 THz can be found in the spectral content of the signal, indicating that the reduced instability increment still exceeds the plasma damping. One can assume that the reduction of the instability increment due to decreased difference between Z_{gs} and Z_{gd} can be compensated by increasing the drift velocity v_0. However, the dramatically increased noise in the signal prevents reliable numerical analysis of the dependence of the threshold drift velocity on the gate position shift.

In Fig. 3(a), new high-frequency sustained plasma modes can be seen in the spectrum above ~14 THz. It is an interference of these modes with the lower frequency modes that produces noticeable noise in the signal. Numerical analysis of the spatial distribution of the electron density in the channel at these high resonant frequencies indicates that these modes are localized in the ungated part of the FET channel between the gate and the drain contact. These modes can result from the DS instability in the ungated asymmetric plasmonic cavities as predicted in Ref. 26. This problem is the subject of our current studies, and the results will be published elsewhere.[27]

Shifting the gate to the middle of the FET channel restores the geometric symmetry, and the DS instability is no longer detected as shown in Fig. 3(b), where the plasmonic signal is damped for both directions of the drift velocity.

At small values of the drift velocity $v_0 \ll v_p$, the DS instability develops in the current-biased plasmonic cavity with ideal boundary conditions ($Z_{gs} = 0$, $Z_{gd} = \infty$) only when $v_0/L_g > 1/\tau$ (the instability threshold).[8,11] Therefore, the instability disappears and plasma oscillations become damped with decreasing drift velocity v_0 and/or relaxation time τ. We numerically analyzed the dependence of the instability threshold on these two parameters for the FET configuration used in Fig. 2(a) with the gate placed in close vicinity to the source contact. In Fig. 4, we show the color map with the regions corresponding to the damped and sustained plasma oscillations in the $v_0 - \tau$ phase space. The theoretical boundary between these two regions under the ideal boundary conditions is shown by the dashed line. From this calculation, it follows that, in general, the instability threshold is close to the "ideal" theoretical value. Deviations from the ideal behavior can be attributed to the finite values of the terminating impedances Z_{gs} and Z_{gd} and their dependence on the resonant plasma frequency. This

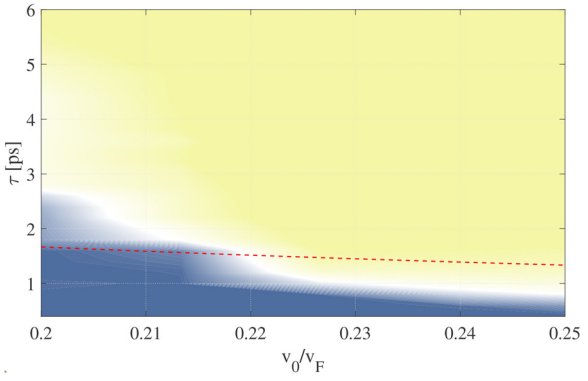

FIG. 4. Color map with regions of damped (blue) and sustained (yellow) plasma oscillations in the $v_0 - \tau$ phase space for the graphene FET with a shifted gate ($x_L = 20$ nm). All other parameters are the same as in Fig. 2. The dashed line shows the instability threshold in the FET with ideal boundary conditions.

result emphasizes the critical importance of the boundary conditions for experimental observation of the DS instability.

The results presented in this paper demonstrate the possibility of the DS plasma instability in the current-biased graphene FET structures with the gate shifted from the middle of the FET channel. We show that the geometric asymmetry is sufficient to trigger the DS plasma instability. We also analyzed the dependence of the strength of sustained plasma oscillations developed in the instability end point on the position of the gate, drift velocity, and the electron relaxation time. It turns out that the strength of the plasmonic resonance (and therefore the power of the radiated THz EM signal) is maximized when the gate is positioned next to the source contact, and the drift velocity is directed toward the drain contact. It is worth mentioning that in the recent publication,[18] the graphene FET with the same geometry and a shifted gate was successfully used for the detection of THz EM radiation. Our results indicate that a similar structure can be used for the generation of THz radiation and potentially lead to the development of tunable on-chip THz sources operating at room temperatures.

This work was partially supported by the Air Force Office of Scientific research (AFOSR) under Grant No. FA9550-16-1-0188 and the U.S. National Science Foundation under Grant No. CNS-2011411.

AUTHOR DECLARATIONS

Conflict of Interest

The authors have no conflicts to disclose.

Author Contributions

Justin Crabb: Data curation (lead); Formal analysis (equal); Methodology (equal); Software (equal); Validation (equal); Writing – original draft (lead). **Xavier Cantos Roman:** Software (supporting); Validation (equal). **Josep Miquel Jornet:** Conceptualization (equal); Funding acquisition (equal); Project administration (equal). **Gregory Aizin:** Conceptualization (lead); Investigation (lead); Methodology (equal); Project administration (lead); Supervision (equal); Writing – review & editing (lead).

DATA AVAILABILITY

The data that support the findings of this study are available within the article.

REFERENCES

[1]E. J. Oughton, W. Lehr, K. Katsaros, I. Selinis, D. Bubley, and J. Kusuma, "Revisiting wireless internet connectivity: 5G vs Wi-Fi 6," Telecommun. Policy **45**, 102127 (2021).
[2]I. F. Akyildiz, C. Han, Z. Hu, S. Nie, and J. M. Jornet, "Terahertz band communication: An old problem revisited and research directions for the next decade," IEEE Trans. Commun. **70**, 4250–4285 (2022).
[3]S. Abadal, E. Alarcón, A. Cabellos-Aparicio, M. C. Lemme, and M. Nemirovsky, "Graphene-enabled wireless communication for massive multicore architectures," IEEE Commun. Mag. **51**, 137–143 (2013).
[4]I. F. Akyildiz and J. M. Jornet, "The internet of nano-things," IEEE Wireless Commun. **17**, 58–63 (2010).
[5]I. F. Akyildiz and J. M. Jornet, "Electromagnetic wireless nanosensor networks," Nano Commun. Networks **1**, 3–19 (2010).
[6]S. Boubanga-Tombet, W. Knap, D. Yadav, A. Satou, D. B. But, V. V. Popov, I. V. Gorbenko, V. Kachorovskii, and T. Otsuji, "Room-temperature amplification of terahertz radiation by grating-gate graphene structures," Phys. Rev. X **10**, 031004 (2020).
[7]Y. Dong, L. Xiong, I. Phinney, Z. Sun, R. Jing, A. McLeod, S. Zhang, S. Liu, F. Ruta, H. Gao *et al.*, "Fizeau drag in graphene plasmonics," Nature **594**, 513–516 (2021).
[8]M. Dyakonov and M. Shur, "Shallow water analogy for a ballistic field effect transistor: New mechanism of plasma wave generation by dc current," Phys. Rev. Lett. **71**, 2465–2468 (1993).
[9]M. Nafari, G. R. Aizin, and J. M. Jornet, "Plasmonic HEMT terahertz transmitter based on the Dyakonov-Shur instability: Performance analysis and impact of nonideal boundaries," Phys. Rev. Appl. **10**, 064025 (2018).
[10]C. B. Mendl, M. Polini, and A. Lucas, "Coherent terahertz radiation from a nonlinear oscillator of viscous electrons," Appl. Phys. Lett. **118**, 013105 (2021).
[11]J. Crabb, X. Cantos-Roman, J. M. Jornet, and G. R. Aizin, "Hydrodynamic theory of the Dyakonov-Shur instability in graphene transistors," Phys. Rev. B **104**, 155440 (2021).
[12]M. Cheremisin and G. Samsonidze, "D'yakonov-Shur instability in a ballistic field-effect transistor with a spatially nonuniform channel," Semiconductors **33**, 578–585 (1999).
[13]D. Svintsov, "Exact solution for driven oscillations in plasmonic field-effect transistors," Phys. Rev. Appl. **10**, 024037 (2018).
[14]W. Knap, J. Lusakowski, T. Parenty, S. Bollaert, A. Cappy, V. Popov, and M. Shur, "Terahertz emission by plasma waves in 60 nm gate high electron mobility transistors," Appl. Phys. Lett. **84**, 2331–2333 (2004).
[15]A. El Fatimy, N. Dyakonova, Y. Meziani, T. Otsuji, W. Knap, S. Vandenbrouk, K. Madjour, D. Théron, C. Gaquiere, M. Poisson *et al.*, "AlGaN/GaN high electron mobility transistors as a voltage-tunable room temperature terahertz sources," J. Appl. Phys. **107**, 024504 (2010).
[16]B. Barut, X. Cantos-Roman, J. Crabb, C.-P. Kwan, R. Dixit, N. Arabchigavkani, S. Yin, J. Nathawat, K. He, M. D. Randle *et al.*, "Asymmetrically engineered nanoscale transistors for on-demand sourcing of terahertz plasmons," Nano Lett. **22**, 2674–2681 (2022).
[17]A. S. Petrov and D. Svintsov, "Perturbation theory for two-dimensional hydrodynamic plasmons," Phys. Rev. B **99**, 195437 (2019).
[18]A. Shabanov, M. Moskotin, V. Belosevich, Y. Matyushkin, M. Rybin, G. Fedorov, and D. Svintsov, "Optimal asymmetry of transistor-based terahertz detectors," Appl. Phys. Lett. **119**, 163505 (2021).
[19]R. Bistritzer and A. H. MacDonald, "Hydrodynamic theory of transport in doped graphene," Phys. Rev. B **80**, 085109 (2009).
[20]S. Rudin, "Non-linear plasma oscillations in semiconductor and graphene channels and application to the detection of terahertz signals," Int. J. High Speed Electron. Syst. **20**, 567–582 (2011).
[21]D. Svintsov, V. Vyurkov, S. Yurchenko, T. Otsuji, and V. Ryzhii, "Hydrodynamic model for electron-hole plasma in graphene," J. Appl. Phys. **111**, 083715 (2012).
[22]A. Tomadin and M. Polini, "Theory of the plasma-wave photoresponse of a gated graphene sheet," Phys. Rev. B **88**, 205426 (2013).
[23]D. Svintsov, V. Vyurkov, V. Ryzhii, and T. Otsuji, "Hydrodynamic electron transport and nonlinear waves in graphene," Phys. Rev. B **88**, 245444 (2013).
[24]U. Briskot, M. Schütt, I. V. Gornyi, M. Titov, B. N. Narozhny, and A. D. Mirlin, "Collision-dominated nonlinear hydrodynamics in graphene," Phys. Rev. B **92**, 115426 (2015).
[25]J. Crabb, X. Cantos-Roman, G. R. Aizin, and J. M. Jornet, "Amplitude and Frequency Modulation with an On-chip Graphene-based Plasmonic Terahertz Nanogenerator," in IEEE Transactions on Nanotechnology (IEEE, 2022).
[26]M. Dyakonov and M. S. Shur, "Current instability and plasma waves generation in ungated two-dimensional electron layers," Appl. Phys. Lett. **87**, 111501 (2005).
[27]J. Crabb, X. Cantos-Roman, J. M. Jornet, and G. R. Aizin, private communication.